Folding of the Four-Way RNA Junction of the Hairpin Ribozyme†

Frank Walter,‡ Alastair I. H. Murchie,‡ and David M. J. Lilley*

CRC Nucleic Acid Structure Research Group, Department of Biochemistry, The University of Dundee, Dundee DD1 4HN, U.K.

Received August 31, 1998; Revised Manuscript Received October 12, 1998

ABSTRACT: The hairpin ribozyme consists of two loop-carrying duplexes (called A and B) that are adjacent arms of a four-way junction in its natural context in the viral RNA. We have shown previously that the activity of the ribozyme is strongly influenced by the structure adopted by the junction. In this study, we have used fluorescence resonance energy transfer to analyze the conformation and folding of the isolated four-way junction. Like other four-way RNA junctions, in the absence of added metal ions this junction adopts a square configuration of coaxially stacked arms, based on A on D and B on C stacking. Upon addition of magnesium ions, the junction undergoes an ion-induced transition to an antiparallel conformation. The data are consistent with folding induced by the binding of a single ion, with an apparent association constant in the range of 2000 M^{-1}. Other divalent metal ions (calcium or manganese) can also induce this change in structure; however, sodium ions are unable to substitute for these ions, and are slightly inhibitory with respect to the transition. The loop-free hairpin junction adopts the same stacking conformer as the full ribozyme, but forms a more symmetrical X-shaped structure. In addition, the apparent stoichiometry of structural ion binding is lower for the isolated junction, and the affinity is considerably lower.

The hairpin ribozyme is a small nucleolytic RNA motif found in the negative strand of the satellite RNA of the tobacco ringspot virus (*1*−*3*) and similar plant viruses (*4*). This motif undergoes site-specific self-cleavage in the presence of magnesium ions, which is required for the processing of RNA replicated by a rolling circle process into monomeric 359 nt RNA molecules. These species then undergo circularization (*5*), and this ligation is also catalyzed by the hairpin ribozyme (*1*), leading to an equilibrium between cleavage and ligation (*6*).

Efforts to reduce the hairpin ribozyme to a minimum functional size (*3*, *7*, *8*) have produced a form comprising two duplexes, each of which contains formally unpaired loops (the A and B loops), connected by the covalent continuity of one strand, i.e., a nick, and the great majority of studies of the ribozyme have concentrated on this form. These have shown that the majority of bases (*9*−*11*) and functional groups (*12*−*14*) required for activity are located in the loops. The single-stranded connection between the two duplex regions should act as a flexible hinge, and it has been generally thought that the functional ribozyme is generated by an association between the A and B loops. Thus, the loops have been connected together in a variety of ways, with results suggesting that the ribozyme is active provided that loop−loop interaction can occur (*15*−*20*). Some activity is even possible in trans, when the loop-carrying duplexes are unconnected (*16*, *21*).

We have noted that in its natural context of the viral RNA, the two loop-carrying duplexes are part of a perfect four-way junction (Figure 1), and we have shown that the ribozyme is active in this form (*22*). We have shown previously that four-way junctions [4H junctions (*23*)] in RNA [like those in DNA (*24*); reviewed in ref *25*] adopt a structure in which helical arms are coaxially stacked in a pairwise manner. There are two conformers possible, depending on the alternative choices of stacking partners, but a given sequence tends to adopt one conformer predominantly [we have recently found an exception to this in the case of DNA junctions, where both conformers are equally populated (*26*)]. Comparative gel electrophoretic analysis indicated that the junction of the hairpin ribozyme (without the loops) adopts the stacking conformer that places the arms that would carry the loops in the full ribozyme on different stacked helical pairs, thus making them potentially available to interact with each other (*22*). Using fluorescence resonance energy transfer, we showed that the full ribozyme adopts the same stacking conformer and is folded by addition of magnesium ions to give a close physical approach of the two arms carrying the loops.

Since the conformation and activity of the hairpin ribozyme are dependent on the four-way junction, it is important to have a full understanding of the conformation and folding of this junction. We have therefore carried out a detailed analysis of the folding properties of the hairpin junction in isolation from the internal loops, using fluorescence resonance energy transfer.

RESULTS

FRET Analysis of the Folding of the Loop-Free Hairpin Ribozyme Junction. The global structure and folding of four-way RNA junctions may be studied using fluorescence resonance energy transfer (FRET). With this approach, we compare the efficiency of energy transfer (E_{FRET}) between donor and acceptor fluorophore pairs attached to the ends

† We thank the CRC and BBSRC for financial support.

* To whom correspondence should be addressed. Telephone: (44)-1382-344243. Fax: (44)-1382-201063. E-mail: dmjlilley@bad.dundee.ac.uk.

‡ Joint first authors.

10.1021/bi9821115 CCC: $15.00
Published on Web 11/20/1998

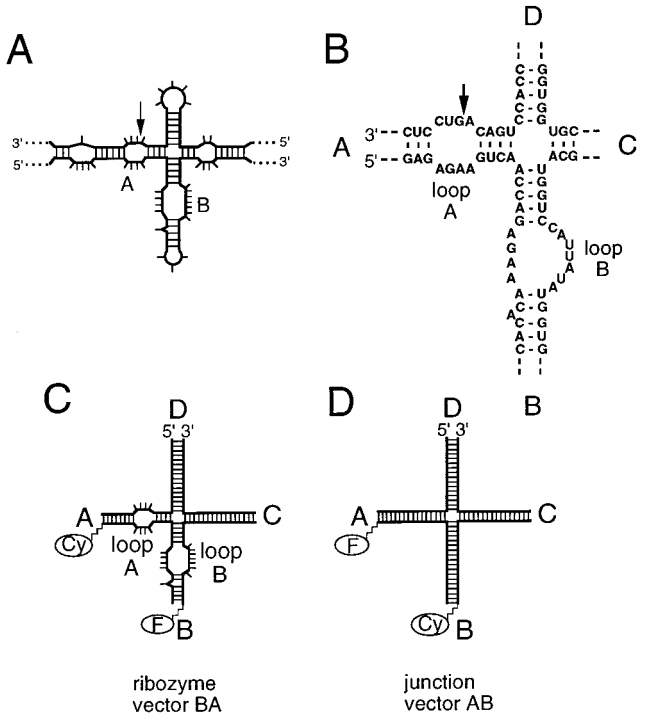

FIGURE 1: Hairpin ribozyme and its four-way RNA junction. (A) Schematic showing the local secondary structure around the hairpin ribozyme of the (−) satellite RNA of the tobacco ringspot virus. The A and B loops are shown, and the position of ribozyme-induced cleavage is indicated by the arrow. (B) The sequence of the hairpin ribozyme and four-way junction (*3*). The arms are named A−D sequentially, beginning with the arms containing the A and B loops. (C) A vector of the hairpin ribozyme for study by FRET. The vectors are named by the arms carrying the fluorophores, in the order donor−acceptor. The example illustrated is vector BA, i.e., $B_{(fluorescein)}-A_{(Cy-3)}$. (D) The AB vector of the four-way junction derived from the hairpin ribozyme.

of different pairs of arms. Since E_{FRET} depends inversely on the separation between the fluorophores (R) according to ref *27*,

$$E_{FRET} = 1/[1 + (R/R_0)^{-6}] \quad (1)$$

where R_0 is the characteristic distance at which $E_{FRET} = 0.5$, the relative distances for the six end-to-end vectors of the four-way junction can be compared in this way. If we base these experiments on a junction with four arms of near-equal length, these end-to-end distances reflect the different angles subtended between the different pairs of helical arms. Because the junction studied in this work is derived from the hairpin ribozyme, three arms are 4 bp shorter than the remaining arm. In our experiments, we employ fluorescein as the donor and indocarbocyanine-3 (Cy3) as the acceptor; these are covalently attached to the 5′ termini of component strands of the junction, thus placing them at the ends of chosen helices. Average labeling efficiencies measured from absorption spectra were 98.5 ± 1.9%. Each helix in the hairpin constructs terminated in a 5′ CC sequence to provide a constant environment for the fluorophores, since we have previously found that this provides a well-behaved environment for FRET measurements in nucleic acids (*28*−*30*). For a given vector, a junction will comprise one strand labeled with fluorescein and one with Cy3 and two unlabeled strands (Figure 1). Each end-to-end distance can be studied in two directions, since the donor and acceptor fluorophores may be exchanged for any given vector.

We perform the FRET analysis using the acceptor normalization approach (*28*, *31*). For each species and set of conditions, we normalize the extracted acceptor spectrum obtained with excitation largely of the donor (490 nm) to a second spectrum excited at 547 nm, where the acceptor absorbs uniquely. The E_{FRET} is readily obtained from this ratio (see Materials and Methods). To interpret this in terms of distance in a straightforward way, it is necessary that one of the fluorophores be flexibly attached to the RNA. Measurement of the anisotropy of the RNA-conjugated fluorophores shows that while Cy3 is constrained ($r = 0.33 \pm 0.01$), the fluorescein is relatively flexible ($r = 0.12 \pm 0.01$).

Our conclusions are derived principally from the comparison of the E_{FRET} values for the six end-to-end distances, using a series of molecules constructed in a very similar manner, and not on the determination of absolute distances.

Global Folding of the Loop-Free Hairpin Ribozyme Junction in the Presence of Magnesium Ions. The junction employed in these studies is derived from the sequence of the hairpin ribozyme (*22*). The nomenclature of arms and strands is equivalent to that used previously in our work (*22*); arms A and B are those that would contain the A and B loops, respectively, in the ribozyme, and arms C and D continue in a circular manner around the junction. Strands a−d are named according to the arm in which their 5′ end is located. The internal loops of the ribozyme were removed by changing the sequence of strand a (thus renamed a′) such that all the bases of strands d and b are complemented. Thus, the junction studied is a perfect 4H junction, with three 16 bp arms (A, C, and D) and one 20 bp arm (B). Fluorescently labeled species are named according to the names of the arms carrying the donor and the acceptor in that order.

The magnitude of E_{FRET} for the six end-to-end vectors of the loop-free hairpin junction in the absence of added metal ions is shown in Figure 2. All the efficiency values are lower than 0.15, indicating the presence of an extended structure. Those of the AD and CB vectors are lower (indicating longer end-to-end distances) than those of the remaining four vectors, consistent with the formation of a 90° crossed structure based on coaxial stacking of A on D and B on C arms. This agrees with our recent analysis by comparative gel electrophoresis (*22*). Upon addition of magnesium ions, the pattern of E_{FRET} values changes: with CD and BA > BD and CA > AD and CB. With 10 mM magnesium ions, the magnitude of E_{FRET} values for CD and BA has reached 0.35, and is significantly greater than that of the remaining four vectors. This suggests that the structure has rotated into an antiparallel conformation, giving the short distances across the A−D and C−B end-to-end vectors. The slightly greater efficiency for the CD vector compared to that for the BA vector could result in part from the longer length of the B arm of the junction.

These conclusions are reinforced by comparing the E_{FRET} values for the six reversed vectors (Figure 2). The patterns obtained in the absence of added ions and in the presence of 10 mM magnesium ions are closely similar to those above, supporting the stacked 90° cross and antiparallel structures, respectively. These reversed vectors required de novo synthesis of fluorophore-labeled RNA and construction of

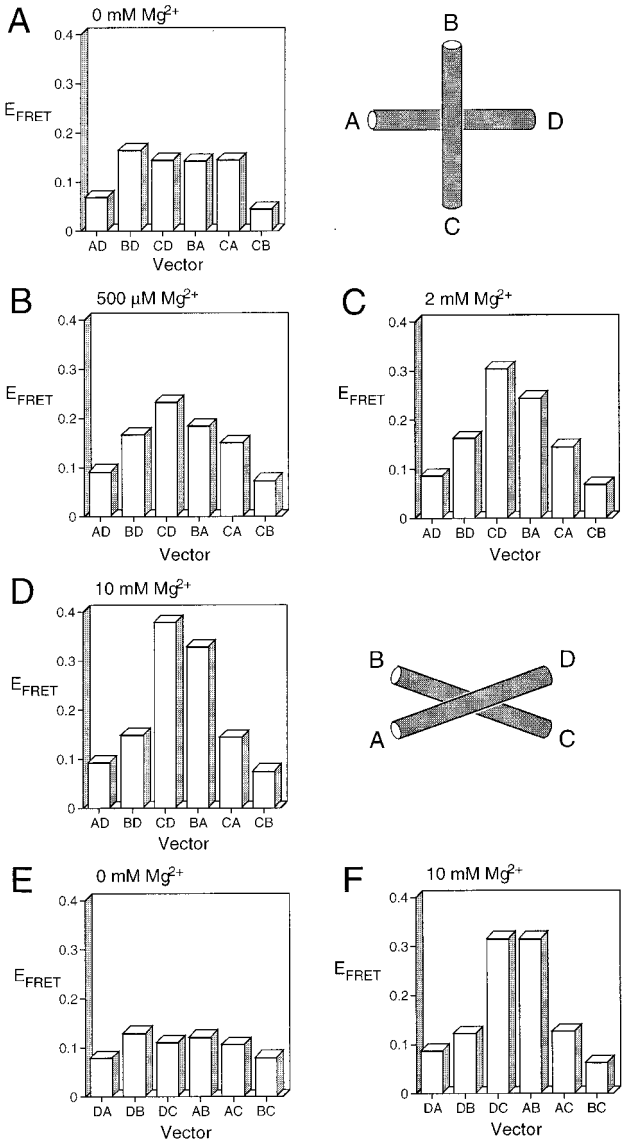

FIGURE 2: Efficiencies of energy transfer for the end-to-end vectors of the loop-free hairpin junction as a function of magnesium ion concentration. In each case, a histogram of E_{FRET} for the six different end-to-end vectors is shown. (A) E_{FRET} values in the absence of added magnesium ions. The pattern of efficiencies is consistent with the schematic model of the global structure shown on the right. This structure is generated by coaxial stacking of A on D and B on C arms, with a 90° angle subtended between the two axes. The resulting structure has four end-to-end distances (AB, BD, DC, and CA) that are slightly shorter than the remaining two (AD and BC), thus explaining the smaller E_{FRET} values for the AD and CB vectors. (B) E_{FRET} values in the presence of 500 μM magnesium ions. (C) E_{FRET} values in the presence of 2 mM magnesium ions. (D) E_{FRET} values in the presence of 10 mM magnesium ions. Under these conditions, the efficiencies can be described by the following: CD $\approx$ BA > BD = CA > AD = CB. These values are consistent with an antiparallel stacked structure based on coaxial stacking of A on D and B on C stacking as indicated schematically on the right. In this structure, the lengths of the end-to-end vectors are described by the following: A−D = B−C > A−C = B−D > A−B = C−D. Note that the handedness of this structure is undetermined, and that implied by the schematic is selected arbitrarily. (E) E_{FRET} values in the absence of added magnesium ions for the reversed set of fluorophore-labeled vectors. As with the first set of vectors (shown in panel A), the pattern of E_{FRET} values is consistent with the extended stacked square structure. (F) E_{FRET} values in the presence of 10 mM magnesium ions for the reversed set of vectors. The pattern is very similar to that found for the first set of vectors (shown in panel D), consistent with the stacked antiparallel structure.

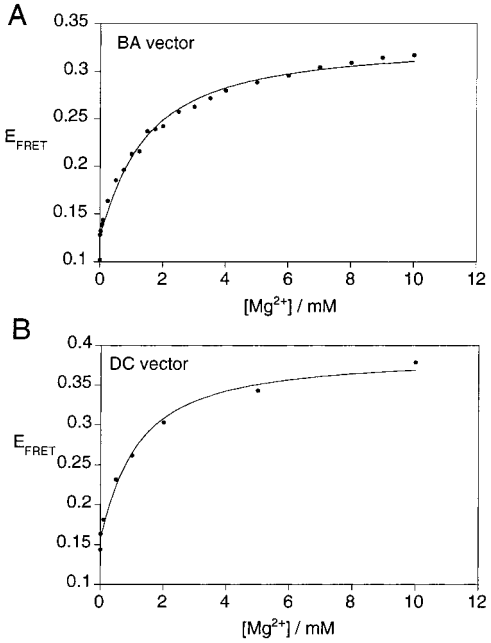

FIGURE 3: Folding of the loop-free hairpin junction over the range of 0−10 mM Mg^{2+} ions followed by the change of E_{FRET} for the short vectors. The experimental data (●) were fitted by regression to a simple binding model where the binding of n ions to the RNA induces a global structural change from the square structure to the antiparallel structure. The lines show the fits to this model for vector BA (A) and DC (B). These data show that the transition to the antiparallel structure is induced by the binding of a single magnesium ion.

new species in which the fluorophores are located differently within the junction. This is therefore a valuable independent confirmation of our structural conclusions, which are also fully in accord with our earlier studies using comparative gel electrophoresis (*22*).

Magnesium Ions Induce Folding by a Single-Ion Binding Mechanism. The ion-induced folding of the loop-free hairpin junction may be followed by studying the increase in E_{FRET} for the shorter distances on titration of magnesium ion concentrations (Figure 3). The data have been fitted (R > 0.993) to a simple empirical model that assumes a two-state conformational transition induced by the binding of n magnesium ions with an apparent association constant K_A:

$$HJ_{90} + nMg^{2+} \leftrightarrow HJ_{AP}\cdot(Mg^{2+})_n$$

where HJ_{90} is the hairpin junction in the stacked 90° cross conformation and HJ_{AP} is that in the antiparallel conformation. According to this simple model, the proportion of junction in the antiparallel form (α) will be given by

$$\alpha = K_A[Mg^{2+}]^n/(1 + K_A[Mg^{2+}]^n) \qquad (2)$$

Values of n were obtained that were close to unity (1.13 ± 0.15 for vector BA and 1.12 ± 0.29 for vector DC), indicative of a noncooperative transition. These values are consistent with a fluorescence-detected transition induced by the binding of a single magnesium ion. Using a single ion binding model, we obtain values for the apparent association constant K_A of 807 and 635 M^{-1} for vectors DC and BA, respectively.

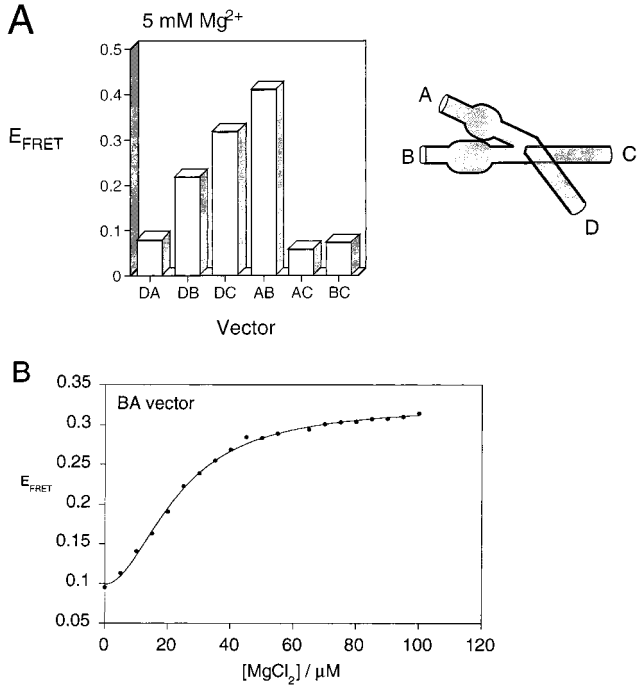

FIGURE 4: Magnesium-induced folding of hairpin ribozyme, complete with the unpaired loops. These data may be compared with those for the simple junction. (A) Histogram of E_{FRET} values for the six different end-to-end vectors in the presence of 5 mM magnesium ions. The pattern of efficiencies is as follows: AB > DC > DB > DA, AC, and BC, consistent with the folded structure shown on the right. This structure is based on the antiparallel structure (in the A on B, D on C stacking conformer) distorted by an interaction between the A and B loops. (B) Folding of the hairpin ribozyme over the range 0−100 μM Mg^{2+} ions followed by the change of E_{FRET} for the shortest vector. The experimental data (●) were fitted by regression to a simple binding model where the binding of n ions to the RNA induces a global structural change from the square structure to the antiparallel structure. The line shows the fit to this model for vector BA. These data show that the transition to the antiparallel structure may be well fitted by a model that requires the binding of two magnesium ions to generate the FRET-observable change in conformation.

Comparison of the Folding of the Isolated Junction and the Full Ribozyme. While the loop-free hairpin junction clearly folds into a fairly symmetrical antiparallel structure in a single-ion-induced transition, we have previously found that the hairpin ribozyme (complete with the A and B loops) folds into a distorted structure in a more complicated ion-induced transition. In Figure 4, we show some additional ribozyme data for comparison with the simple junction (*22*). Since the d strand contains a 2′-deoxyriboadenine substitution at the cleavage site in all our constructs, this species is unable to catalyze strand cleavage. In the presence of 5 mM magnesium ions, the hairpin ribozyme exhibits a pattern of E_{FRET} values that is a distorted form of the antiparallel pattern (Figure 4A), such that the efficiency for vector AB is greater than that for DC and the value for vector DB is significantly elevated. We have interpreted this pattern to indicate a distortion of the structure caused by close association of the A and B loops. Titration of the E_{FRET} for the BA vector (Figure 4B) shows that the ion dependence is more complex than the single-ion-induced transition of the isolated junction. The shape of the curve suggests cooperative ion binding is responsible for inducing the transition. The fitted value of n is close to 2 ($n = 1.96 \pm 0.1$). While strictly speaking this value is a Hill coefficient, the value would be consistent with a mechanism requiring the binding of two ions ($n = 1.96 \pm 0.1$) before the transition is detected. Folding of the complete ribozyme is induced by a lower magnesium ion concentration, with an apparent association constant K_A of 1.9×10^9 M^{-2} calculated for a two-ion binding model.

Global Folding of the Loop-Free Hairpin Ribozyme Junction in the Presence of Calcium and Manganese Ions. Magnesium ions are not unique in their ability to fold the loop-free hairpin junction. Comparison of the six end-to-end vectors in the presence of calcium and manganese ions (Figure 5) shows that the structure formed is closely similar in each case to that induced by magnesium ions. Titration of calcium and manganese ions (Figure 5) shows that they also induce folding in an apparent single-ion binding mode ($n = 1.06$ for Ca^{2+} and 1.31 for Mn^{2+}, both followed by the CD vector). The apparent association constant (calculated for single-ion binding) for the calcium ion-induced folding was 1,208 M^{-1}, while that for manganese ion was 642 M^{-1}.

Sodium Ions Do Not Induce Formation of the Antiparallel Structure. Magnesium, calcium, and manganese ions are all divalent ions. By contrast, monovalent ions are generally less effective in promoting structural transitions in nucleic acids, and the hairpin junction is no exception to this. The comparison of E_{FRET} values for the six end-to-end vectors as a function of the sodium ion level reveals no formation of the pattern indicating the antiparallel structure (Figure 6A). By contrast, in the presence of sodium ions, the pattern remains indicative of an extended conformation, but with a distortion consistent with rotation into a parallel structure. We have previously described a parallel conformation for four-way RNA junctions in the presence of sodium ions (*32*).

The addition of 50 mM sodium ions to a junction poised at the point of folding by 500 μM magnesium ions (compare with Figure 2B) fails to induce further folding in the antiparallel direction (Figure 6B); if anything, folding is inhibited. However, addition of a sufficiently high magnesium ion concentration can overcome any inhibition by sodium ions. Thus, the hairpin junction is clearly folded into the antiparallel structure in the presence of a mixture of 10 mM sodium and 10 mM magnesium ions (Figure 6C). However, in the presence of this concentration of sodium ions, the folding is a more complex function of magnesium ion concentration compared to the single-ion binding for the pure divalent ions.

We sought further evidence for the structure of the hairpin junction in the presence of sodium ions using an alternative technique, that of comparative gel electrophoresis. With this method, we construct all six species of a chosen four-way junction in which two arms are significantly longer than the remaining two. We compare the electrophoretic mobility of these six species in polyacrylamide, and analyze the results on the assumption that the mobility will reflect the angle subtended between the longer arms. Because it is presently difficult to synthesize RNA molecules of the required length, we construct junctions where the central core of 10 bp on each arm is made of RNA, and the remaining part is composed of DNA. We thus made the six extended junctions of the hairpin junction, having two longer 40 bp arms and two shorter 15 bp arms.

In the presence of 2 mM magnesium ions, the pattern of electrophoretic mobilities may be described by fast, inter-

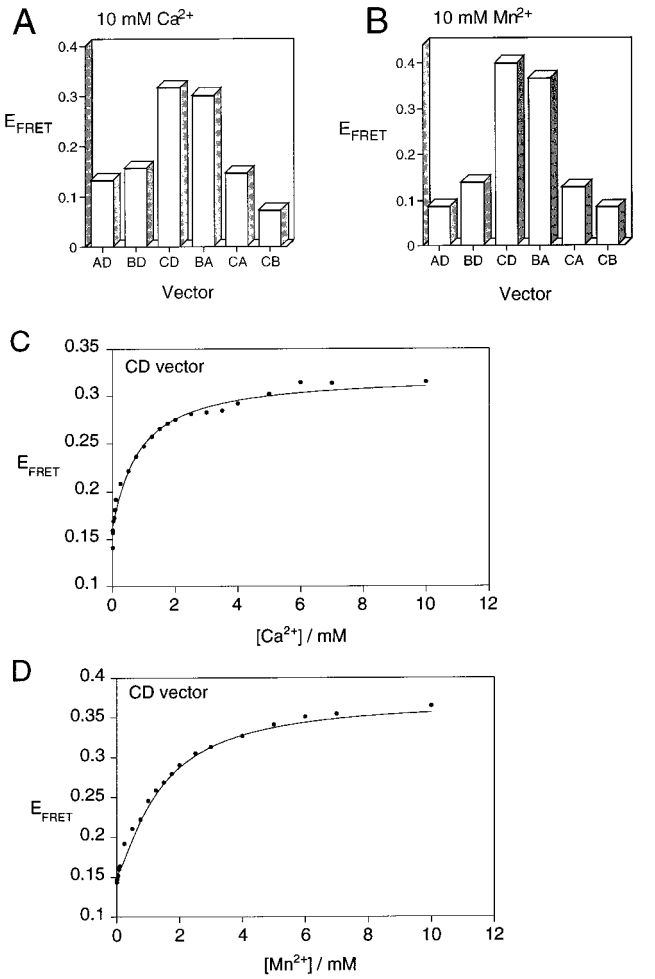

FIGURE 5: Folding of the loop-free hairpin junction in the presence of other divalent metal ions. The E_{FRET} values for the six different end-to-end vectors were studied in calcium and manganese ions, and the folding studied by the change in E_{FRET} for the short CD vector. (A) Histogram of E_{FRET} values for the end-to-end vectors in the presence of 10 mM calcium ions. The pattern of efficiencies is closely similar to that observed in the presence of 10 mM magnesium ions (Figure 2D), indicating that calcium ions induce the folding into the same antiparallel structure. (B) Histogram of E_{FRET} values for the end-to-end vectors in the presence of 10 mM manganese ions. Once again, the pattern of efficiencies is very similar to those observed in the presence of 10 mM magnesium or calcium ions, indicating that manganese ions also induce the folding into the antiparallel structure. (C) Folding of the loop-free hairpin junction over the range of 0−10 mM Ca^{2+} ions followed by the change of E_{FRET} for the short CD vector. Fitting the experimental data (●) indicates that the folding into the antiparallel structure is induced by the binding of a single calcium ion. (D) Folding of the loop-free hairpin junction over the range of 0−10 mM Mn^{2+} ions followed by the change of E_{FRET} for the CD vector. As with magnesium and calcium ions, fitting the experimental data (●) indicates that the folding is induced by the binding of a single manganese ion.

mediate, slow, slow, intermediate, fast (Figure 7A), consistent with the antiparallel stacked X structure. This is in agreement with earlier electrophoretic analysis (*22*), and the FRET results presented here. In contrast, in the presence of sodium ions as the only added cation, the pattern of mobilities is fast, slow, fast, fast, slow, fast (Figure 7B). This pattern has been observed before in a four-way RNA junction. It is not straightforward to analyze, but may be interpreted in terms of the formation of a parallel stacked structure, consistent with our present FRET results (compare with Figure 6A).

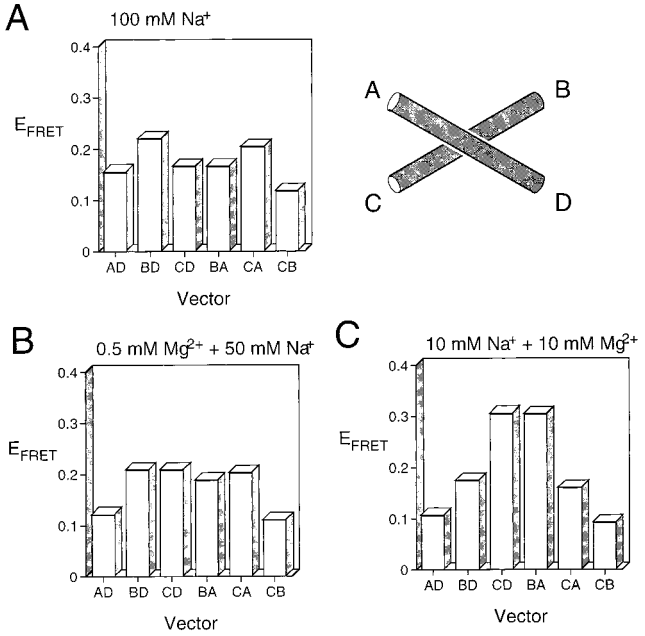

FIGURE 6: Global structure of the loop-free hairpin junction in the presence of sodium ions. The E_{FRET} values for the six different end-to-end vectors were studied in the presence of sodium ions alone and as mixtures with magnesium ions. (A) Histogram of E_{FRET} values for the end-to-end vectors in the presence of 100 mM sodium ions. The pattern of efficiencies is consistent with some distortion into a parallel structure (indicated schematically at the right) such that the shortest vectors are the BD and CA end-to-end distances. (B) Histogram of E_{FRET} values for the end-to-end vectors in the presence of 50 mM sodium and 500 μM magnesium ions. Under these conditions, the pattern of efficiencies is consistent with the 90° crossed structure illustrated in Figure 2A. Comparison with the pattern obtained in the presence of 500 μM magnesium ions alone (Figure 2B) indicates that the sodium ions inhibit the folding into the antiparallel conformation. (C) Histogram of E_{FRET} values for the end-to-end vectors in the presence of 10 mM sodium and 10 mM magnesium ions. The pattern is clearly that of the antiparallel structure (compare with Figure 2D), despite the presence of the additional sodium ions.

In the presence of 1 mM magnesium and 10 mM sodium ions (Figure 7C), the pattern of mobilities becomes fast, slow, slow, slow, slow, fast. This is consistent with a square, stacked structure, in good agreement with the FRET analysis (Figure 6B).

DISCUSSION

In its natural context, the hairpin ribozyme consists of the familiar two loop-bearing duplexes displayed on the framework of a perfect four-way helical junction. We have shown that in its global structure and folding this junction behaves as a typical 4H RNA junction.

In the absence of added metal ions, the junction adopts the stacked 90° cross structure, based on the pairwise coaxial stacking of A on D and B on C arms, where the two helical axes are mutually perpendicular. In the presence of sodium ions, this undergoes a rotation in the direction of a parallel structure. While these properties are similar to those of other four-way RNA junctions studied in this laboratory (*32*, *33*), they contrast strongly with the conformational properties of four-way DNA junctions. Most strikingly, the RNA junctions fail to undergo the opening into the unstacked, square structure under low-salt conditions that is universal for DNA junctions (*34*−*36*). This difference is likely to arise from

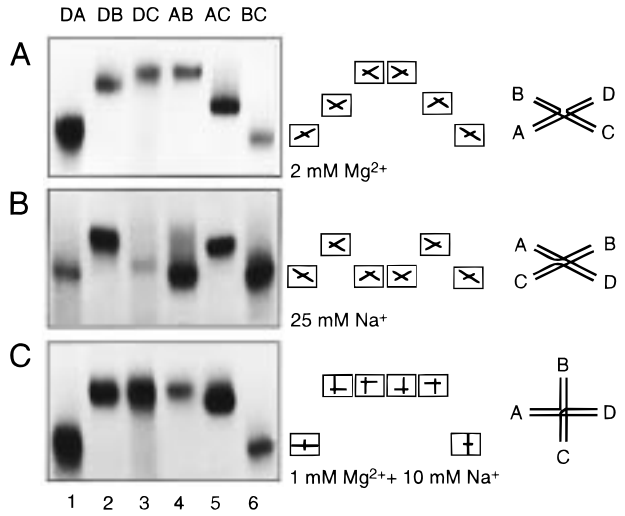

FIGURE 7: Analysis of the global structure of the loop-free hairpin junction in the presence of sodium ions analyzed by comparative gel electrophoresis. Four-way junctions were generated from strands in which the central 20 nucleotides were RNA and the remaining 30 nucleotides at each end were DNA. The six possible species having two long 30 bp arms and two shorter 10 bp arms were created, and named according to the long arms (e.g., species DA has long D and A arms and short B and C arms). The six long−short species were electrophoresed in a polyacrylamide gel in the presence of 90 mM Tris-borate (pH 8.3) with the indicated metal ion concentrations. The junctions were created from strands that were radioactively 5′-^{32}P-labeled, and thus, the different junction species were revealed by autoradiography of dried gels. (A) Analysis in the presence of 2 mM magnesium ions. Under these conditions, the six long−short species give a pattern that is consistent with the antiparallel structure, indicated at the far right. This generates the predicted long−short species shown at the right. (B) Analysis in the presence of 25 mM sodium ions. The six long−short species migrate in a pattern that is most readily explicable in terms of a rotation into a parallel geometry (far right). (C) Analysis in the presence of 1 mM magnesium and 10 mM sodium ions. Under these conditions, the pattern is clearly that of the 90° crossed structure (far right). Lanes contained (1) DA species, (2) DB species, (3) DC species, (4) AB species, (5) AC species, and (6) BC species.

the different helical geometry of the component arms, which adopt the A-form structure in RNA compared to the B-form structure for the DNA helices. This could alter steric relationships, and will give a different spatial distribution of charges which may therefore change the energetic balance between electrostatic repulsion and coaxial helical stacking.

Upon addition of divalent metal ions, the loop-free hairpin junction undergoes a change in global structure in which the angle between the two helical axes rotates to adopt an antiparallel geometry. Although more complex schemes could be consistent with the data, this transition can be empirically well fitted as a two-state process, induced by the binding of a single magnesium, calcium, or manganese ion. The rotation brings helices A and B into relatively close proximity, which is required in the case of the full ribozyme to achieve interaction between the two loops. Sodium ions are unable to promote this transition, or to augment the effect of divalent ions; if anything, they are slightly inhibitory with respect to folding induced by magnesium ions and induce a rotation in the opposite sense toward the parallel structure. Despite these metal ion-induced changes to the global structure, the marked preference for A on D stacking remains constant throughout. The conformational changes are summarized schematically in Figure 8.

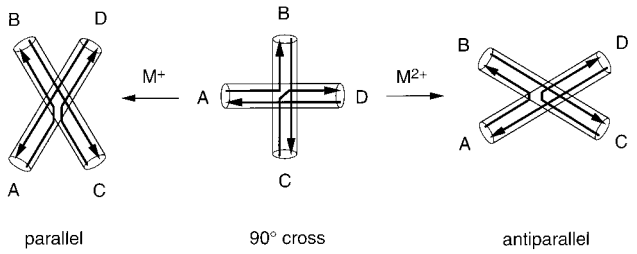

FIGURE 8: Summary of the global folding of the four-way junction of the hairpin ribozyme. The junction is folded by pairwise coaxial stacking of A on D and B on C arms under all conditions examined, but the angle between the two helical axes varies with the type and concentration of metal ions present. In the absence of added metal ions, the junction adopts the 90° cross (center), where the axes are approximately perpendicular. Addition of divalent metal ions in the millimolar range induces a rotation into an antiparallel geometry (right), while addition of sodium ions appears to cause a rotation in the opposite sense, into what is most readily interpreted in terms of a parallel structure (left). The 5′ to 3′ polarity of the component strands is indicated by the arrows.

It is interesting to compare the folding of the loop-free hairpin junction to that of the full ribozyme, including the loops (*22*). In the absence of added divalent metal ions, both species adopt the same stacked 90° crossed structure, and under these conditions, there is no interaction possible between the loops of the ribozyme. Both species adopt the same stacking conformer (based on A on D stacking), indicating that the overall folding of the ribozyme is determined by the stacking preference of the junction. We have recently demonstrated that the activity of the ribozyme in its four-way junction form is affected by the conformation of the junction (*22*).

Upon addition of divalent metal ions, the folding properties of the full ribozyme are different from those of the isolated junction in a number of respects. First, the full ribozyme is less symmetrical than the simple junction. In the hairpin ribozyme, the end-to-end distances can be summarized AB < DC < DB, suggesting a global structure that is distorted by close interaction between the A and B loops that pulls these arms together. Second, the FRET-observed transition to the antiparallel structure can be analyzed as a multiple-ion-induced process, in contrast to the single-ion-induced transition for the isolated junction. Last, the apparent affinities for the divalent ions are very different between the loop-free junction, which becomes folded in the millimolar range, and the full ribozyme, where folding is induced by metal ions with a concentration in the micromolar range.

Taken together, these results are consistent with a model in which folding of the hairpin ribozyme is induced by the binding of two ions. These could be distributed between the four-way junction, which binds one ion, and the interface between the loops, which could bind a second structural ion. Thus, in the absence of the internal loops, we observe the folding of the junction alone induced by the binding of a single ion. Moreover, in the absence of the junction (i.e., the hinged form of the ribozyme), there is also ion-induced association between the loops (*37*) (F. Walter, A. I. H. Murchie, and D. M. J. Lilley, unpublished data). Folding of the complete ribozyme may be interpreted in terms of a requirement for the binding of both ions before the FRET-detected transition occurs. Rotation into the antiparallel structure allows the two loops to dock together, which is

presumably integral to the catalytic function, and the strong interaction between these regions distorts the global symmetry of the junction.

MATERIALS AND METHODS

Synthesis of RNA. DNA−RNA oligonucleotides were synthesized using phosphoramidite chemistry (*38*) implemented on Applied Biosystems 394 synthesizers. RNA was synthesized using ribonucleotide phosphoramidites with 2′-*tert*-butyldimethylsilyl (TBDMS) protection (*39*, *40*) (Glen Research). 6-Fluorescein (PE-ABI) and Cy3 (Glen Research) were coupled to the 5′ termini as phosphoramidites. Oligoribonucleotides were deprotected in a 25% ethanol/ammonia solution at 55 °C for 6 h (dye-labeled) or 12 h (unlabeled) and evaporated to dryness. Oligoribonucleotides were redissolved in 0.5 mL of 1 M tetrabutylammonium fluoride (TBAF, Aldrich) in tetrahydrofuran to remove TBDMS groups and agitated at 20 °C in the dark for 16 h prior to desalting by G25 Sephadex (NAP columns, Pharmacia) and ethanol precipitation. Fully deprotected oligonucleotides were purified by gel electrophoresis in 20% polyacrylamide containing 7 M urea; fluorescently labeled species were significantly retarded in the gel system. Bands were excised, and the oligonucleotides were electroeluted into 8 M ammonium acetate and recovered by ethanol precipitation. Fluorescently labeled oligonucleotides were dissolved in 100 mM ammonium acetate and applied to a C18 reversed phase HPLC column (μBondapak, Waters). RNA was eluted with a linear gradient of acetonitrile; buffer A was 100 mM ammonium acetate and buffer B acetonitrile, with a flow rate of 1 mL/min. The peak fractions were evaporated to dryness, redissolved in water, and then ethanol precipitated. Absorption spectra of fluorescently labeled RNA were recorded on a Cary 1E UV−visible spectrometer.

Construction of Fluorescently Labeled Hairpin Junctions. Each fluorescent junction species for FRET studies was constructed by hybridizing stoichiometric quantities of the four appropriate RNA oligonucleotides in 90 mM Tris-borate (pH 8.3) and 25 mM NaCl for 10 min at 65 °C, followed by slow cooling. The hybridized junctions were loaded onto an 8% polyacrylamide gel and electrophoresed at 4 °C for 22 h at 150 V. The buffer system contained 90 mM Tris-borate (pH 8.3) and 25 mM NaCl and was recirculated at >1 L/h. Fluorescent junctions were visualized by direct exposure to a standard lamp; the bands were excised, and the RNA was electroeluted into 8 M ammonium acetate and recovered by ethanol precipitation.

Fluorescence Spectroscopy. Fluorescence spectra were recorded at 5 °C in 90 mM Tris-borate (pH 8.3) with the required concentrations of added metal ions. Spectroscopy was performed on an SLM-Aminco 8100 fluorimeter operating in the photon counting mode, and spectra were corrected for lamp fluctuations and instrumental variations as described in ref *41*. Spectra were recorded with excitation and emission polarizers set at a relative angle of 54.74° to avoid polarization artifacts. FRET efficiencies were measured using the acceptor normalization method (*28*, *31*) in which an extracted acceptor spectrum $F^A(\nu_1,\nu')$ (excitation at a ν' of 490 nm, with emission at ν_1) is normalized to a further spectrum $[F(\nu_2,\nu'')]$ excited at a wavelength ($\nu'' = 547$ nm) at which only the acceptor absorbs, with emission at ν_2. The acceptor ratio is calculated with

$$(\text{ratio})_A = F^A(\nu_1,\nu')/F(\nu_2,\nu'') = \{E_{FRET}d^+[\epsilon^D(\nu')/\epsilon^A(\nu'')] + [\epsilon^A(\nu')/\epsilon^A(\nu'')]\} \times [\Phi^A(\nu_1)/\Phi^A(\nu_2)] \quad (3)$$

Superscripts D and A refer to donor and acceptor, respectively. ϵ^D and ϵ^A are the molar absorption coefficients at the indicated frequency of donor and acceptor, respectively, and Φ^A is the fluorescent quantum yield of the acceptor. $\epsilon^D(\nu')/\epsilon^A(\nu'')$ and $\epsilon^A(\nu')/\epsilon^A(\nu'')$ are measured from absorption spectra; $\Phi^A(\nu_1)/\Phi^A(\nu_2)$ is unity when $\nu_1 = \nu_2$, and thus, E_{FRET} can be calculated directly from $(\text{ratio})_A$. Fluorescence anisotropy values (r) were determined from measurements of fluorescence intensity using vertical excitation and emission polarizers ($F_{||}$) and vertical excitation and horizontal emission polarizers ($F_\perp$, corrected for variation in detection sensitivity). Fluorescence anisotropy was calculated from

$$r = (F_{||} - F_\perp)/(F_{||} + 2F_\perp) \quad (4)$$

FRET experiments were performed on junctions assembled from oligonucleotides of the following sequences (all written 5′ to 3′):

a′ strand CCGCACAGGACUGUCAACCAGGUAAUAUAACCACCGG
b strand CCGGUGGUAUAUUACCUGGUACGCCUUGACGUGGGG
c strand CCCCACGUCAAGGCGUGGUGGCCGAAGGUCGG
d strand CCGACCUUCGGCCACCUGACAGUCCUGUGCGG

Underlined nucleotides are deoxynucleotides. The construct that included the A and B loops was derived by replacing the a′ strand with the following sequence:

a strand CCGCACAGAGAAGUCAACCAGAGAAACACACCGG

Comparative Gel Electrophoresis. This was carried out exactly as described by Duckett et al. (*32*). Sixteen DNA−RNA oligonucleotides were synthesized, of which the four longest had the following sequences:

CGCAAGCGACAGGAACCTCGAGGGATCCGTUUCGGCCACCUGACAGUCCUGGAAGCTTCTC
GAGGTTCCTGTCGCTTGCG
CGCAAGCGACAGGAACCTCGAGAAGCTTCCAGGACUGUCAACCAGGUAAUTTGAATTCCTC
GAGGTTCCTGTCGCTTGCG
CGCAAGCGACAGGAACCTCGAGGAATTCAAAUUACCUGGUACGCCUUGACAGTCTAGACTC
GAGGTTCCTGTCGCTTGCG
CGCAAGCGACAGGAACCTCGAGTCTAGACTGUCAAGGCGUGGUGGCCGAAACGGATCCCTC
GAGGTTCCTGTCGCTTGCG

The sequences of the remaining 12 oligonucleotides can be derived by deletion of 25 nucleotides at the 5′, 3′, or both termini.

ACKNOWLEDGMENT

We are grateful to Drs. G. S. Bassi and R. M. Clegg for valuable discussion and Ms. Audrey Gough for skilled technical assistance.

REFERENCES

1. Buzayan, J. M., Gerlach, W. L., and Bruening, G. (1986) *Nature 323*, 349−353.

2. Feldstein, P. A., Buzayan, J. M., and Bruening, G. (1989) *Gene 82*, 53−61.
3. Hampel, A., and Tritz, R. (1989) *Biochemistry 28*, 4929−4933.
4. DeYoung, M. B., Siwkowski, A. M., Lian, Y., and Hampel, A. (1995) *Biochemistry 34*, 15785−15791.
5. van Tol, H., Buzayan, J. M., and Bruening, G. (1991) *J. Virol. 280*, 23−30.
6. Hegg, L. A., and Fedor, M. J. (1995) *Biochemistry 34*, 15813−15828.
7. Hampel, A., Tritz, R., Hicks, M., and Cruz, P. (1990) *Nucleic Acids Res. 18*, 299−304.
8. Chowrira, B. M., Berzal-Herranz, A., and Burke, J. M. (1991) *Nature 354*, 320−322.
9. Berzal-Herranz, A., Simpson, J., Chowrira, B. M., Butcher, S. E., and Burke, J. M. (1993) *EMBO J. 12*, 2567−2574.
10. Anderson, P., Monforte, J., Tritz, R., Nesbitt, S., Hearst, J., and Hampel, A. (1994) *Nucleic Acids Res. 22*, 1096−1100.
11. Siwkowski, A., Shippy, R., and Hampel, A. (1997) *Biochemistry 36*, 3930−3940.
12. Chowrira, B. M., Berzal-Herranz, A., Keller, C. F., and Burke, J. M. (1993) *J. Biol. Chem. 268*, 19458−19462.
13. Grasby, J. A., Mersmann, K., Singh, M., and Gait, M. J. (1995) *Biochemistry 34*, 4068−4076.
14. Schmidt, S., Beigelman, L., Karpeisky, A., Usman, N., Sorensen, U. S., and Gait, M. J. (1996) *Nucleic Acids Res. 24*, 573−581.
15. Komatsu, Y., Koizumi, M., Nakamura, H., and Ohtsuka, E. (1994) *J. Am. Chem. Soc. 116*, 3692−3696.
16. Butcher, S. E., Heckman, J. E., and Burke, J. M. (1995) *J. Biol. Chem. 270*, 29648−29651.
17. Komatsu, Y., Kanzaki, I., and Ohtsuka, E. (1996) *Biochemistry 35*, 9815−9820.
18. Komatsu, Y., Kanzaki, I., Shirai, M., and Ohtsuka, E. (1997) *Biochemistry 36*, 9935−9940.
19. Komatsu, Y., Shirai, M., Yamashita, S., and Ohtsuka, E. (1997) *Bioorg. Med. Chem. 5*, 1063−1069.
20. Earnshaw, D. J., Masquida, B., Müller, S., Sigurdsson, S. T., Eckstein, F., Westhof, E., and Gait, M. J. (1997) *J. Mol. Biol. 274*, 197−212.
21. Shin, C., Choi, J. N., Sang, S. I., Song, J. T., Ahn, J. H., Lee, J. S., and Choi, Y. D. (1996) *Nucleic Acids Res. 24*, 2685−2689.
22. Murchie, A. I. H., Thomson, J. B., Walter, F., and Lilley, D. M. J. (1998) *Mol. Cell 1*, 873−881.
23. Lilley, D. M. J., Clegg, R. M., Diekmann, S., Seeman, N. C., von Kitzing, E., and Hagerman, P. (1995) *Eur. J. Biochem. 230*, 1−2.
24. Duckett, D. R., Murchie, A. I. H., Diekmann, S., von Kitzing, E., Kemper, B., and Lilley, D. M. J. (1988) *Cell 55*, 79−89.
25. Lilley, D. M. J., and Clegg, R. M. (1993) *Annu. Rev. Biophys. Biomol. Struct. 22*, 299−328.
26. Grainger, R. J., Murchie, A. I. H., and Lilley, D. M. J. (1998) *Biochemistry 37*, 23−32.
27. Förster, T. (1948) *Ann. Phys. 2*, 55−75.
28. Murchie, A. I. H., Clegg, R. M., von Kitzing, E., Duckett, D. R., Diekmann, S., and Lilley, D. M. J. (1989) *Nature 341*, 763−766.
29. Clegg, R. M., Murchie, A. I. H., Zechel, A., Carlberg, C., Diekmann, S., and Lilley, D. M. J. (1992) *Biochemistry 31*, 4846−4856.
30. Clegg, R. M., Murchie, A. I. H., Zechel, A., and Lilley, D. M. J. (1993) *Proc. Natl. Acad. Sci. U.S.A. 90*, 2994−2998.
31. Clegg, R. M. (1992) *Methods Enzymol. 211*, 353−388.
32. Duckett, D. R., Murchie, A. I. H., and Lilley, D. M. J. (1995) *Cell 83*, 1027−1036.
33. Walter, F., Murchie, A. I. H., Duckett, D. R., and Lilley, D. M. J. (1998) *RNA 4*, 719−728.
34. Duckett, D. R., Murchie, A. I. H., and Lilley, D. M. J. (1990) *EMBO J. 9*, 583−590.
35. Duckett, D. R., and Lilley, D. M. J. (1991) *J. Mol. Biol. 221*, 147−161.
36. Clegg, R. M., Murchie, A. I. H., Zechel, A., and Lilley, D. M. J. (1994) *Biophys. J. 66*, 99−109.
37. Walter, N. G., Hampel, K. J., Brown, K. M., and Burke, J. M. (1998) *EMBO J. 17*, 2378−2391.
38. Beaucage, S. L., and Caruthers, M. H. (1981) *Tetrahedron Lett. 22*, 1859−1862.
39. Hakimelahi, G. H., Proba, Z. A., and Ogilvie, K. K. (1981) *Tetrahedron Lett. 22*, 5243−5246.
40. Perreault, J.-P., Wu, T., Cousineau, B., Ogilvie, K. K., and Cedergren, R. (1990) *Nature 344*, 565−567.
41. Bassi, G. S., Murchie, A. I. H., Walter, F., Clegg, R. M., and Lilley, D. M. J. (1997) *EMBO J. 16*, 7481−7489.

BI9821115